ICMNS 2021, 30 June 2021

Cortical functional architectures and contact geometry

Jean Petitot,
CAMS, EHESS, Paris,
jean.petitot@ehess.fr

1. Introduction

Neurogeometry concerns integrative and functional neurosciences.

It works at the mesoscopic level and does not directly concern the ODEs of neurons and PDEs of neural networks.

Its purpose is rather to understand the cortical implementation of the *global geometry* of visual percepts as resulting from an *integration* process of retinal very local ("differential") sense data.

2. Point-like processors

This purpose comes up against a "hard problem".

The *geometry* of visual perception involves many *differential* computations. But neurons are *point-like processors*. They can only code a single numerical value by means of their "firing rate".

Of course they are connected and they can transmit their activity along their more or less inhibitory or excitatory connections.

But this is insufficient to *directly* implement differential routines.

3. The antinomy of perceptual geometry. I

There is therefore an *antinomy* at the root of a neurally implemented perceptual geometry.

How differential routines can be neurally implemented in networks of "point-like processors" since derivatives are not point-like entities?

4. The hard problem

Now, it is a key empirical fact that biological evolution has introduced *new* post-retinal neural modules and neural layers (lateral geniculate nucleus, cortical layers, orientation hypercolumns, etc.) that implement *new* variables beyond variables of retinal position .

We can therefore try to understand how a connectivity *extended* to these new modules and layers can perform differential computations.
(i) It must certainly have a *very special* functional architecture.
(ii) But we must also know under what conditions a point-like functional architecture is able to implement a differential calculus.

5. The antinomy of perceptual geometry. II

The hypothesis is therefore

Maybe point-like processors can implement an alternative formulation of differential calculus using "hidden derivatives" (Richard Montgomery) as new supplementary independent variables which can be implemented in point-like processors.

But these new "hidden" derivatives must satisfy strong *constraints* in order to be interpretable as "true" derivatives.

For that, *the connectivity of the network must be extremely specific*.

6. The antinomy of perceptual geometry. III

Now, alternative versions of differential calculus do exist in "modern" differential geometry since Pfaff, Jacobi, Frobenius, Lie, Darboux, Cartan, Weyl, Goursat, etc.

They can solve the "hard problem".

To understand why, we have to dive deep into the history of differential geometry.

7. Geometrizing integrability I

The geometrization of the integrability conditions of differential equations has been a revolution (similar to that accomplished by Galois for the resolution of algebraic equations).

For a long time, the problem of the integration of differential equations $\omega = \sum_{i=1}^{i=n} A_i dx_i = 0$ was considered as "impossible", "absurd", "meaningless" if there was no integrating factor.

Gaspard Monge (1746-1818) was one of the first to explain (1784) that (in dimension 3) the conditions of integrability mean that the solutions of $\omega = 0$ are *surfaces* $F(x_i) = a$ in $\mathbb{R}^3$ but that, when the conditions are not satisfied, there still exist solutions but which are 1D *skew curves* and no longer 2D surfaces.

8. Geometrizing integrability II

From Pfaff to Frobenius differential geometers had gradually understood the condition of integrability $\omega \wedge d\omega = 0$.

Monge raised what became 30 years later the Pfaff problem and he prophesied its importance.

> *"It was not noticed that this was the beginning of an immense chain, to which lay the great difficulties of differential calculus."*

From that moment, geometrizing the integrability of differential equations became the problem of analyzing *tangent hyperplane fields* (kernels of differential 1-forms).

So, the basic notion became that of a *contact element* (Lie's "Flächen-element") , that is a pair of a point x of a manifold M and a hyperplane K_x of T_xM.

Sophus Lie developed it in great detail with a strong sense of the inversion of point of view it brought.

In a beautiful text of 1894 "The Geometric Work of Sophus Lie", Felix Klein emphasized the importance of the change of perspective brought about with this "new, clear and penetrating view".

He explained that Lie introduced "new elements of space" much more general than points and, instead of applying the methods of differential analysis to geometry, was interested in "the reciprocal" and developed "the application of geometrical intuition to Analysis".

This is the key foundational issue: the essence of differential calculus moves from Analysis to Geometry.

So, we see why and how "point-like processors" can be good differential geometers if they are able to detect contact elements.

11. The first example: $V1$

In the 90s I developped the following relations between neurophysiology and geometry:

1. a class of cortical neurons in $V1$ (called "simple") detect contact elements (a, p) where a are positions on the retina and p a local orientation at a (Hubel and Wiesel);
2. the fibration $(a, p) \longrightarrow a$ is neurophysiologically implemented by retinotopy and orientation hypercolumns;
3. the contact structure of the 1-jets of plane curves is neurophysiologically implemented (horizontal cortico-cortical connections);
4. the sub-Riemannian geometry of this contact structure is neurophysiologically implemented (illusory contours as geodesics).

12. Illusory contours

By the way, long range illusory contours are one of the most striking phenomenon of low level vision. We can reconstruct the shape of a dalmatian dog in this very incomplete image:

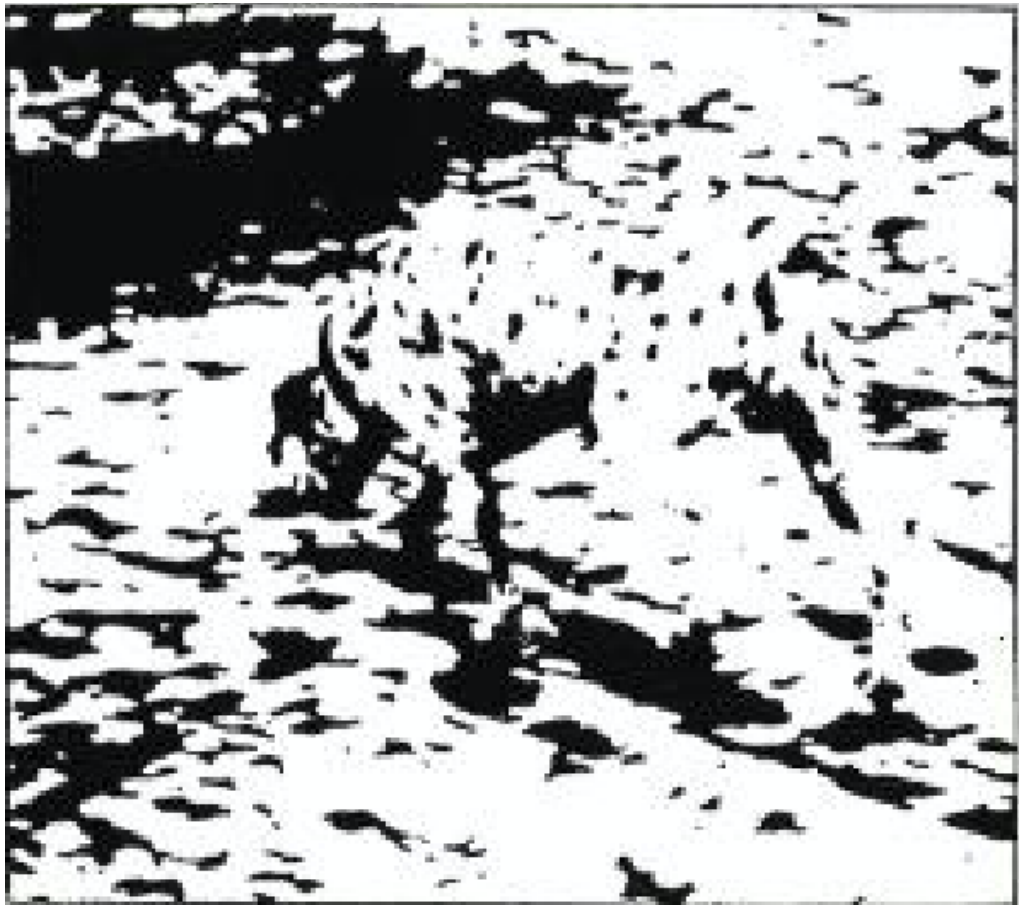

13. Illusory contours as geodesics

We will see that they can be interpreted as *geodesics* of a contact structure for an appropriate metric.

Such sub-Riemannian models generalize a previous model due to David Mumford and based on the theory of *elastica*.

They have many applications, in particular for *inpainting*, since to complete a corrupted image, we must construct the *illusory level sets* that can complete the missing parts.

14. An example of sub-Riemannian inpainting

The following picture shows how a highly corrupted image (left) can be very well restored using sub-Riemannian diffusion (Gauthier-Prandi inpainting).

The face of our friend Jean-Paul appears out of the blue.

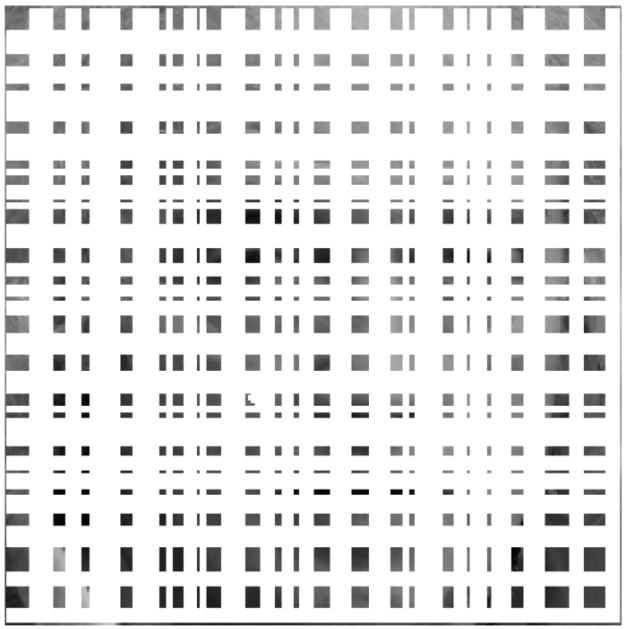

15. The functional architecture

Simple neurons of $V1$ are parametrized by triples (a, p) where $a = (x, y)$ is a position on the retina (identified with $\mathbb{R}^2$) and p is an orientation (modulo π) at a.

So, simple cells of $V1$ constitute a *field of orientations*.

This field is the basis of the "functional architecture" of $V1$.

What could be its structure?

16. Braitenberg abduction

The first global reconstruction of an orientation field from the sparse local data provided by electrodes (Hubel and Wiesel) was *infered* abductively in 1979 by Valentino and Carla Braitenberg.

This was long before the introduction of modern *in vivo* optical imaging techniques.

17. Swindale's abduction

After Braitenberg, in an astonishing 1987 paper (still before the advent of optical imaging techniques), Nicholas Swindale reconstructed the "spatial layout" of the orientation map.

What are now called *pinwheels*.

He thus confirmed Braitenberg's abduction.

18. Swindale's image I

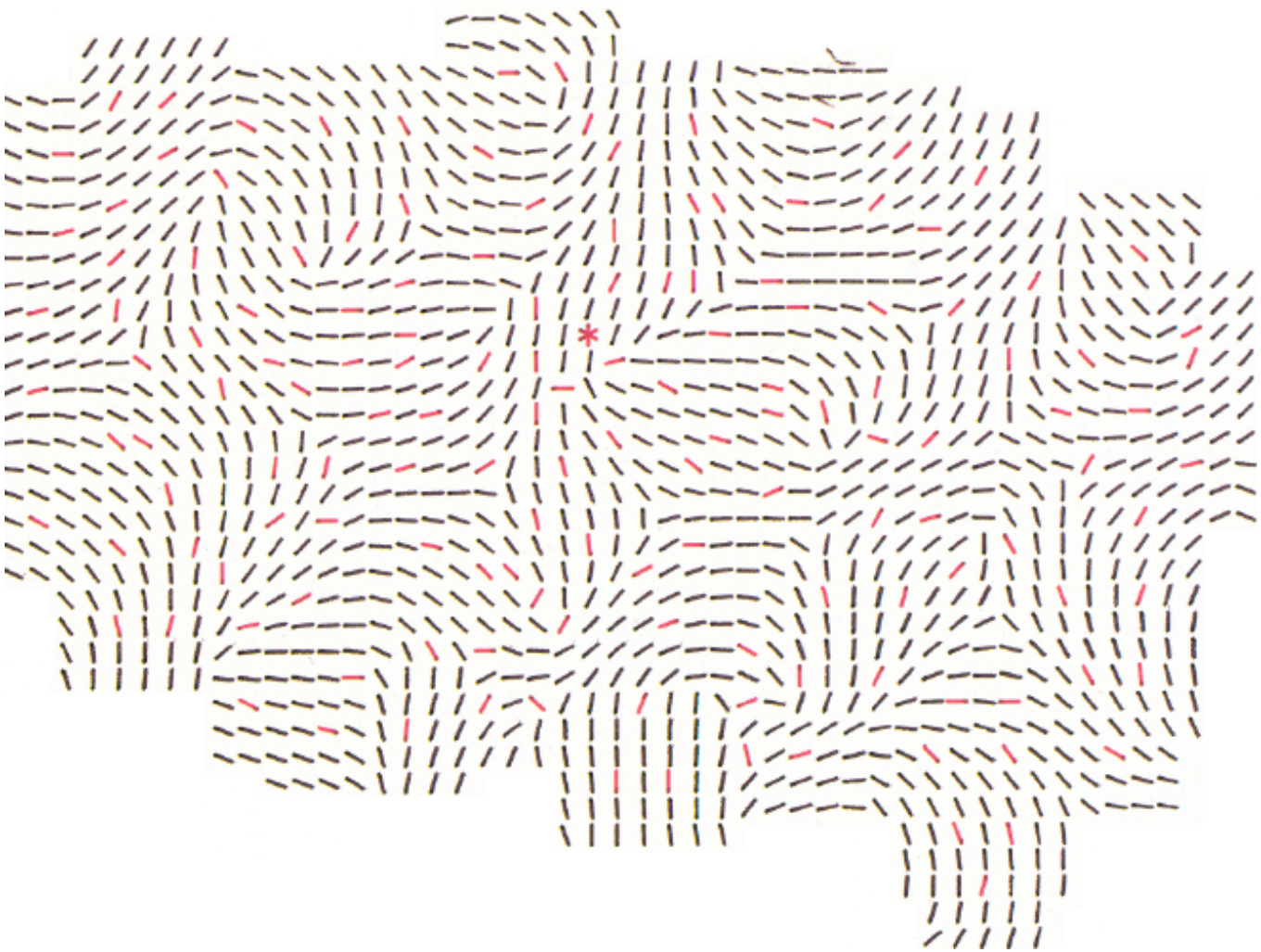

19. Swindale's image II

Using a color code for directions, he got an orientation map.

This is a theoretical reconstruction and not an empirical observation.

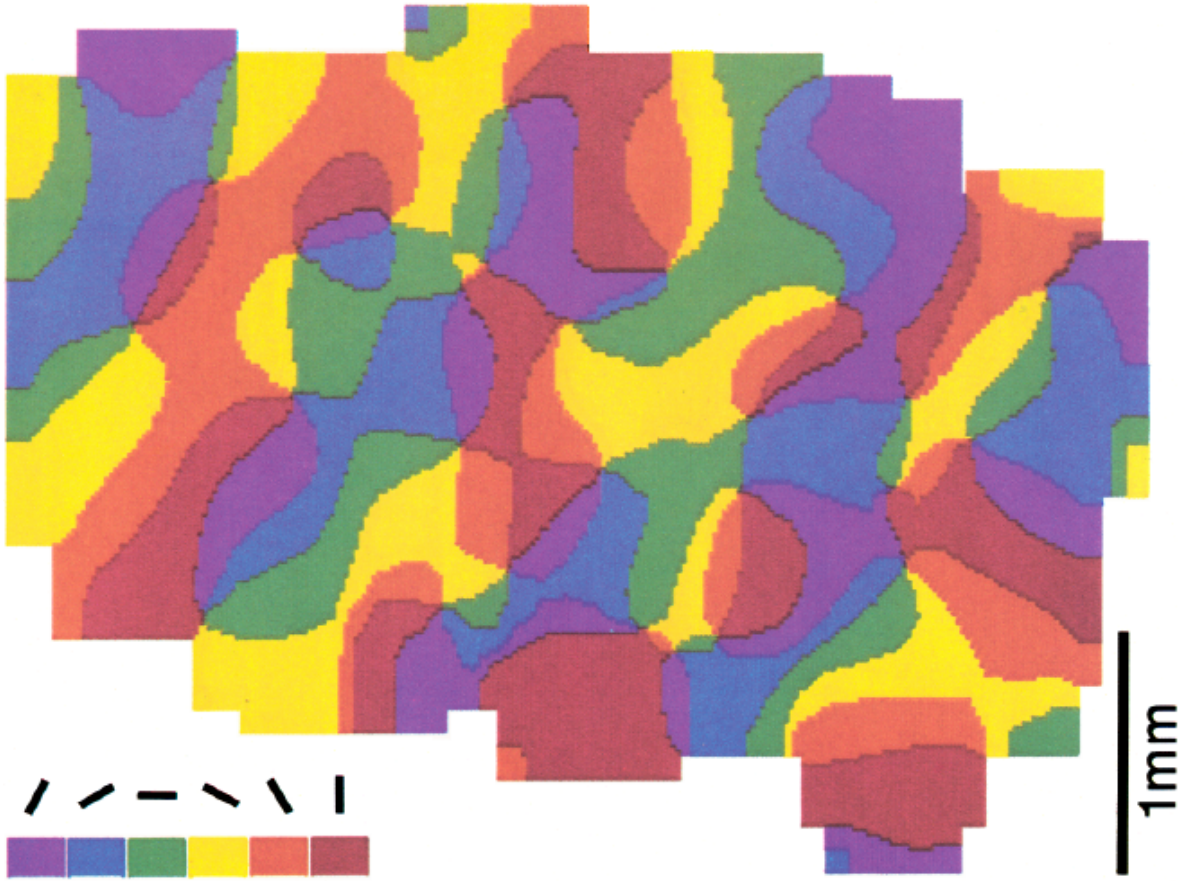

20. In vivo optical imaging

Braitenberg's and Swindale's abductions have been strikingly confirmed in the 1990s by brain imagery (Amiram Grinvald and Tobias Bonhöffer). You all know orientations maps with pinwheels (here $V1$ area of the macaque, Blasdel and Salama).

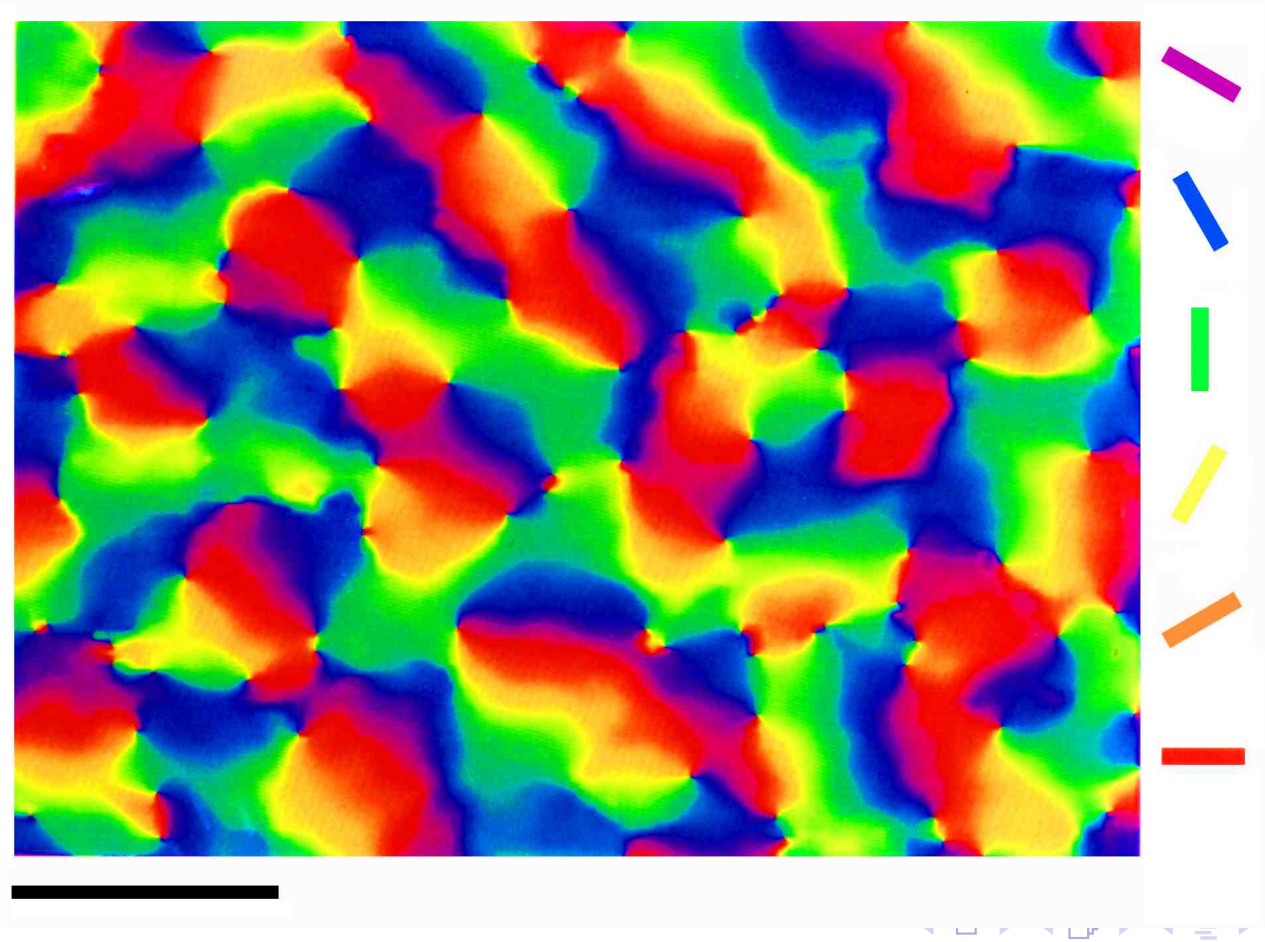

21. Pinwheels as blowing-up

Pinwheels can be interpreted geometrically as *blowing-up* of points a_i and the orientation field is the closure of a section σ of the fiber bundle $\pi : \mathbb{V}_J = \mathbb{R}^2 \times \mathbb{P}^1 \to \mathbb{R}^2$ (J for "jets") defined over the open subset $\mathbb{R}^2 - \{a_i\}$.

Over the a_i the closure of σ is the "exceptionnal" fiber $\mathbb{P}^1_{a_i}$.

These exceptional fibers $\mathbb{P}^1_{a_i}$ are "contracted" and "folded" onto small neighborhoods of the base points a_i.

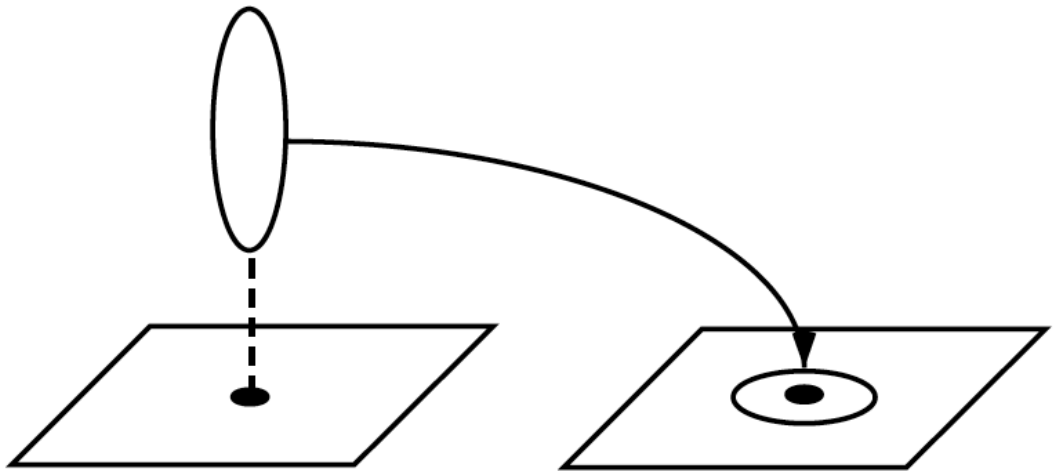

22. V1 as fiber bundle

There is therefore a $3D \to 2D$ dimensional collapse : an orientation map is, in a way, a geometric object of "intermediate" dimension between 2 and 3.

At the limit, when all the points of the base plane $\mathbb{R}^2$ are blown-up in parallel, we get the fiber bundle $\pi : \mathbb{V}_J = \mathbb{R}^2 \times \mathbb{P}^1 \to \mathbb{R}^2$.

So $\mathbb{V}_J$ can be considered as an *idealized continuous model* of the concrete neural $V1$ produced by biological evolution with it pinwheels and orientation field.

23. "Hidden derivatives"

But the fibration $\mathbb{V} = \mathbb{R}^2 \times \mathbb{P}^1 \longrightarrow \mathbb{R}^2, (a, p) \mapsto a$ is not sufficient for interpreting p as an "hidden derivative" (Richard Montgomery), that is as a tangent to a curve.

For that, p must satisfy the fundamental Pfaff equation $\omega = dy - pdx = 0$ defining the contact structure of 1-jets of plane curves.

24. The contact structure of 1-jets

A skew curve

$$\Gamma = v(s) = (a(s), p(s)) = (x(s), y(s), p(s))$$

in $\mathbb{V}_J$ is the *Legendrian lift* of its projection $\gamma = a(s)$ onto the base plane $\mathbb{R}^2$

- iff it is an *integral curve* of the *contact structure* $\mathcal{C} = ker(\omega)$ of $\mathbb{V}_J$, where ω is the 1-form

$$\omega = dy - pdx$$

25. The (polarized) Heisenberg group

Let's remember that the contact structure $\mathcal{C}$ is left-invariant for a group law making $\mathbb{V}_J$ isomorphic to the (*polarized*) *Heisenberg group* $\mathbb{H}_{pol}$.

$$(x, y, p).(x', y', p') = (x + x', y + y' + px', p + p') \ .$$

Its Lie algebra is generated by the basis of left-invariant fields $X_1 = \frac{\partial}{\partial x} + p\frac{\partial}{\partial y} = (1, p, 0)$ and $X_2 = \frac{\partial}{\partial p} = (0, 0, 1)$ with $[X_1, X_2] = (0, -1, 0) = -\frac{\partial}{\partial y} = -X_3$ (the other brackets $= 0$).

The basis $\{X_1, X_2\}$ of the distribution $\mathcal{C}$ is *bracket generating* (*i.e.* Lie-generates the whole tangent bundle $T\mathbb{V}_J$) (Hörmander condition).

$\mathbb{V}_J = \mathbb{H}_{pol}$ is a *nilpotent* group of step 2 (a Carnot group).

26. The contact structure of $SE(2)$

This can be generalized to the Euclidean group $SE(2)$.

The contact form of $SE(2)$ is

$$\omega_S = \cos(\theta)\, dy - \sin(\theta)\, dx$$

The contact planes are spanned by the tangent vectors $X_1 = \cos(\theta)\frac{\partial}{\partial x} + \sin(\theta)\frac{\partial}{\partial y}$ and $X_2 = \frac{\partial}{\partial \theta}$ with Lie bracket $[X_1, X_2] = \sin(\theta)\frac{\partial}{\partial x} - \cos(\theta)\frac{\partial}{\partial y} = -X_3$.

27. The two models

The X_j constitute an Euclidean orthonormal basis.

The distribution $\mathcal{C}$ of contact planes is still bracket generating (Hörmander condition). But $SE(2)$ is no longer nilpotent. The Carnot group $\mathbb{V}_J = \mathbb{H}_{pol}$ is its "*tangent cone*", its "nilpotentisation".

28. Neural contact structure

The very key point, which is another striking *experimental* discovery, is that the contact structure of $\mathbb{V}$ is *implemented* in a *specific class* of neural connections.

Orientation hypercolumns correspond to the "vertical" retino-geniculo-cortical connectivity.

But cortical neurons of $V1$ are also connected by "horizontal" cortico-cortical connections *inside the cortical layer itself*.

29. Necessity of a parallel transport

Such a second system of long-range "horizontal" cortico-cortical connections is necessary to implement a *parallel transport* enabling the visual system to *compare* two retinotopically neighboring orientation hypercolumns P_a and P_b over two different base points a and b.

30. The key result

"The system of long-range horizontal connections can be summarized as preferentially linking neurons with co-oriented, co-axially aligned receptive fields." (W. Bosking)

This means that a chain of simple neurons (a_i, p_i) is a chain of *"horizontally" connected* simple neurons iff it is a discretization of the Legendrian lift of a not too curved base curve interpolating between the (a_i).

So, this means that,

up to some bound on curvature, the contact structure $\mathcal{C}$ is neurally implemented in $V1$.

31. Variational models for illusory contours

Let us come back now to *curved* illusory contours. *Variational models* have been introduced since the late 70s.

They minimize an energy along curves *in the base plane*.

The best known is the *elastica* model proposed in 1992 by David Mumford.

32. Geodesic models

But for *neural* models (and not only 2D image processing) it is natural to work in $V1$, that is with the *contact structure* and the *Legendrian lifts*.

It is here that sub-Riemannian geometry fully comes on stage.

The natural idea is to introduce sub-Riemannian metrics on $\mathbb{V}$ and look at geodesic models for curve completion and illusory modal contours.

33. The sub-Riemannian $\mathbb{H}_{pol}$

The sub-Riemannian geometry of the Heisenberg group $\mathbb{H}$ has been explained in the 1980s by Richard Beals, Bernard Gaveau and Peter Greiner.

It can easily be adapted to the polarized $\mathbb{H}_{pol}$.

As you know, geodesics are the projections on $\mathbb{H}_{pol}$ of the trajectories of a Hamiltonian field defined on the cotangent space.

34. The sub-Riemannian wavefront of $\mathbb{H}$

Using a variable φ, associated to the length of the geodesic, the sphere $S(0,R)$ and the wave front $W(0,R)$ of $\mathbb{H}$ are given by the following equations (where θ is the angle of the tangent)

$$\begin{cases} x_1 = \frac{|\sin(\varphi)|}{\varphi}\cos(\theta) \\ p_1 = \frac{|\sin(\varphi)|}{\varphi}\sin(\theta) \\ y_1 = \frac{1}{2}x_1 p_1 + \frac{\varphi - \sin(\varphi)\cos(\varphi)}{4\varphi^2} \\ = \frac{1}{2}\frac{\sin^2(\varphi)}{\varphi^2}\cos(\theta)\sin(\theta) + \frac{\varphi - \cos(\varphi)\sin(\varphi)}{4\varphi^2} \\ = \frac{\varphi + 2\sin^2(\varphi)\cos(\theta)\sin(\theta) - \cos(\varphi)\sin(\varphi)}{4\varphi^2} \end{cases}$$

They are displayed in the following figure.

Such a complex behavior is impossible in Riemannian geometry.

35. Image of the SR sphere of $\mathbb{H}$

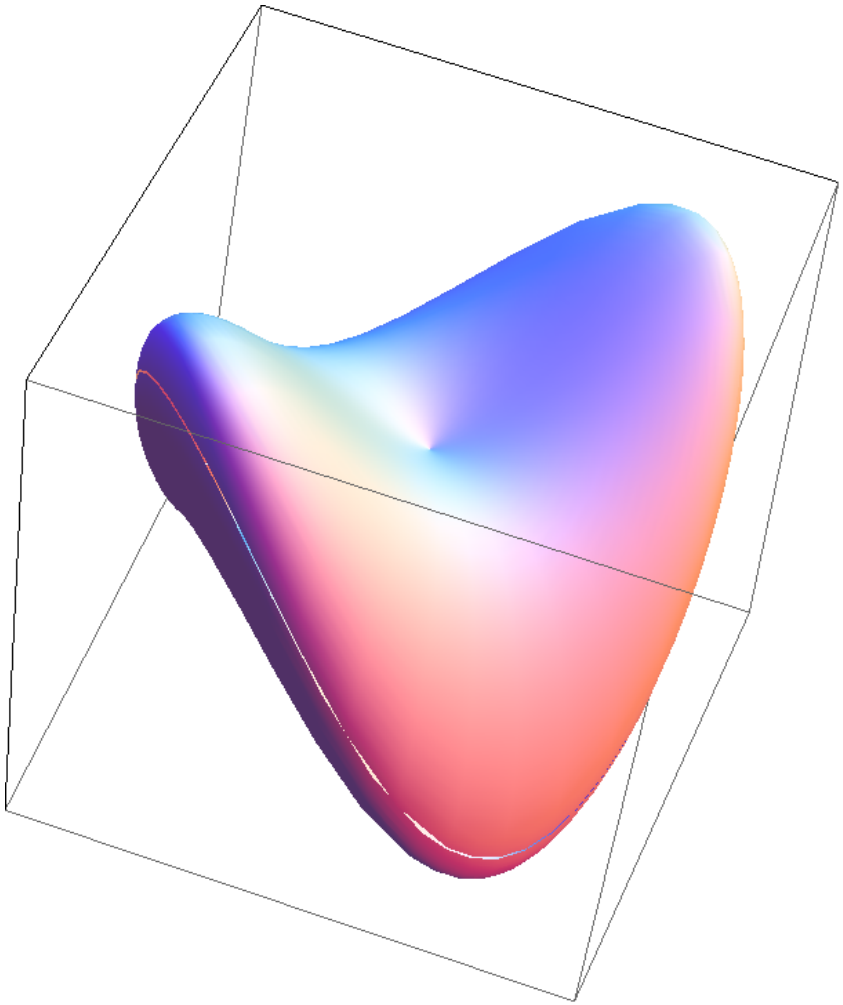

36. Image of the SR sphere and wave-front of $\mathbb{H}$

The external surface is the sub-Riemannian sphere S. It has a saddle form with singularities at the intersections with the y-axis. The internal part is $W - S$. It presents smaller and smaller circles of cusp singularities which converge to 0.

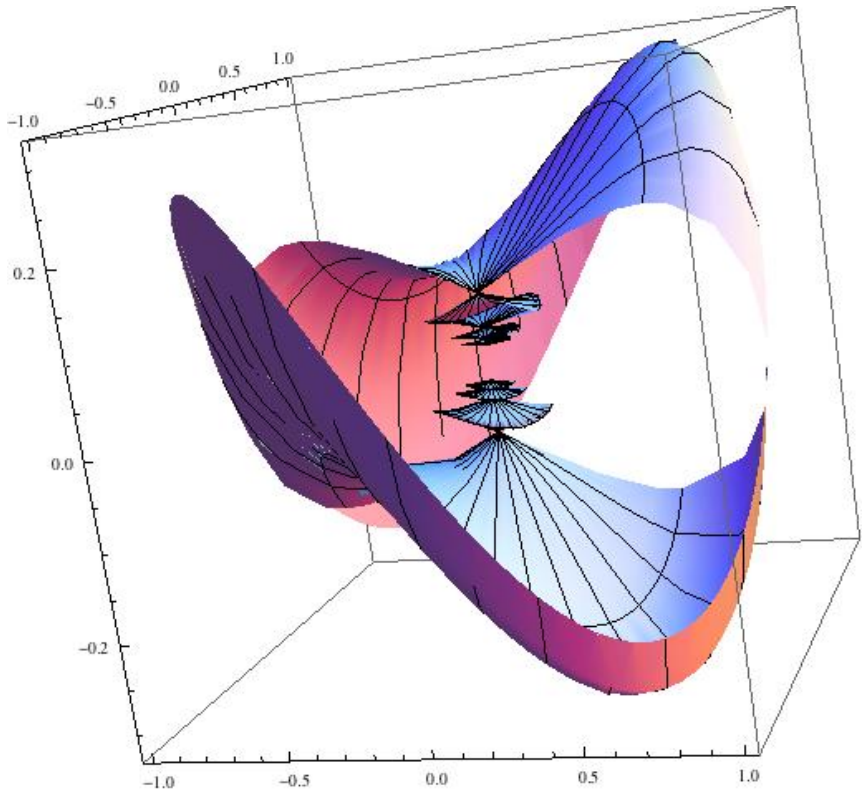

37. The cusps of W

The following figure displays the quarter of the wave front W for $\theta = 0$. Its equations are $x_1 = \frac{|\sin(\varphi)|}{\varphi}$, $p_1 = 0$, $y_1 = \frac{\varphi - \cos(\varphi)\sin(\varphi)}{4\varphi^2}$.
The cusps are on the curve of equation $x = \cos(\varphi)$,
$y = \frac{1}{4}\cos(\varphi)\sin(\varphi)$.

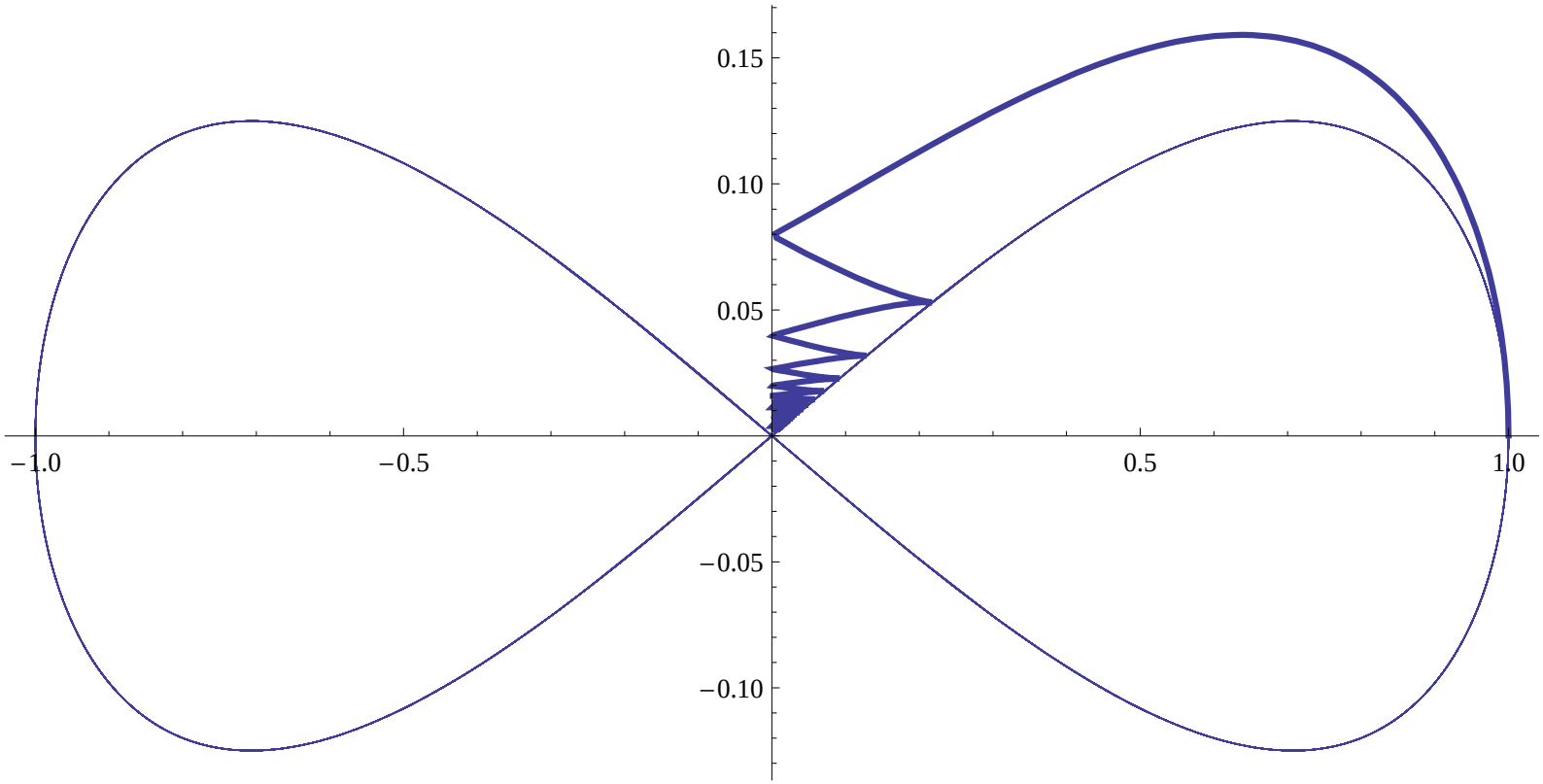

38. The example of $SE(2)$

With Giovanna Citti and Alessandro Sarti we studied the passage from the $\mathbb{V}_J$ bundle, with its natural action of the Euclidean group $\mathbb{R}^2 \rtimes \mathbb{S}^1 = SE(2)$, to its associated principal bundle.

We thus go to the model $SE(2) = \mathbb{V}_S$ endowed with its natural contact structure and its associated L-invariant sub-Riemannian metric.

The geometry of the sub-Riemannian spheres and wavefronts is much more complicated. It was computed in the 2000s by Andrei Agrachev and his team (Yuri Sachkov, Ugo Boscain, Igor Moiseev, Jean-Paul Gauthier).

39. The Hamiltonian of $SE(2)$

If λ_1, λ_2, λ_3 are the components of the covector λ in the bass $(\omega_1, \omega_2, \omega_3)$ dual to (X_1, X_2, X_3) (i.e. $\lambda_i = \langle \lambda, X_i \rangle$), the Hamiltonian giving the geodesics is

$$H(\lambda, q) = \frac{1}{2}\left(\lambda_1^2 + \lambda_2^2\right)$$

If H is constant $H = \frac{1}{2}$ and if we take $\lambda_1 = \sin\left(\frac{\gamma}{2}\right)$, $\lambda_2 = -\cos\left(\frac{\gamma}{2}\right)$, then γ satisfies the *pendulum equation*

$$\ddot{\gamma} = -\sin(\gamma)$$

and Hamilton equations are

$$\begin{cases} \dot{x} = \sin\left(\frac{\gamma}{2}\right)\cos(\theta) = \lambda_1 \cos(\theta) \\ \dot{y} = \sin\left(\frac{\gamma}{2}\right)\sin(\theta) = \lambda_1 \sin(\theta) \\ \dot{\theta} = -\cos\left(\frac{\gamma}{2}\right) = \lambda_2 \\ \ddot{\theta} = \frac{1}{2}\sin\left(\frac{\gamma}{2}\right)\dot{\gamma} = \dot{\lambda}_2 \end{cases}$$

41. The control pendulum

The phase portrait $\mathcal{C}$ of the pendulum is stratified and its stratification governs the classification of geodesics.

42. The pendulum phase portrait

In magenta: open stratum C_1 (2 connected components, oscillations). In yellow: open stratum C_2 (2 connected components, rotation). In thick lines: the 1-dimensional stratum C_3 (4 connected components). Point strata C_4 (2 points, stable equilibrium) and C_5 (2 points, unstable equilibrium).

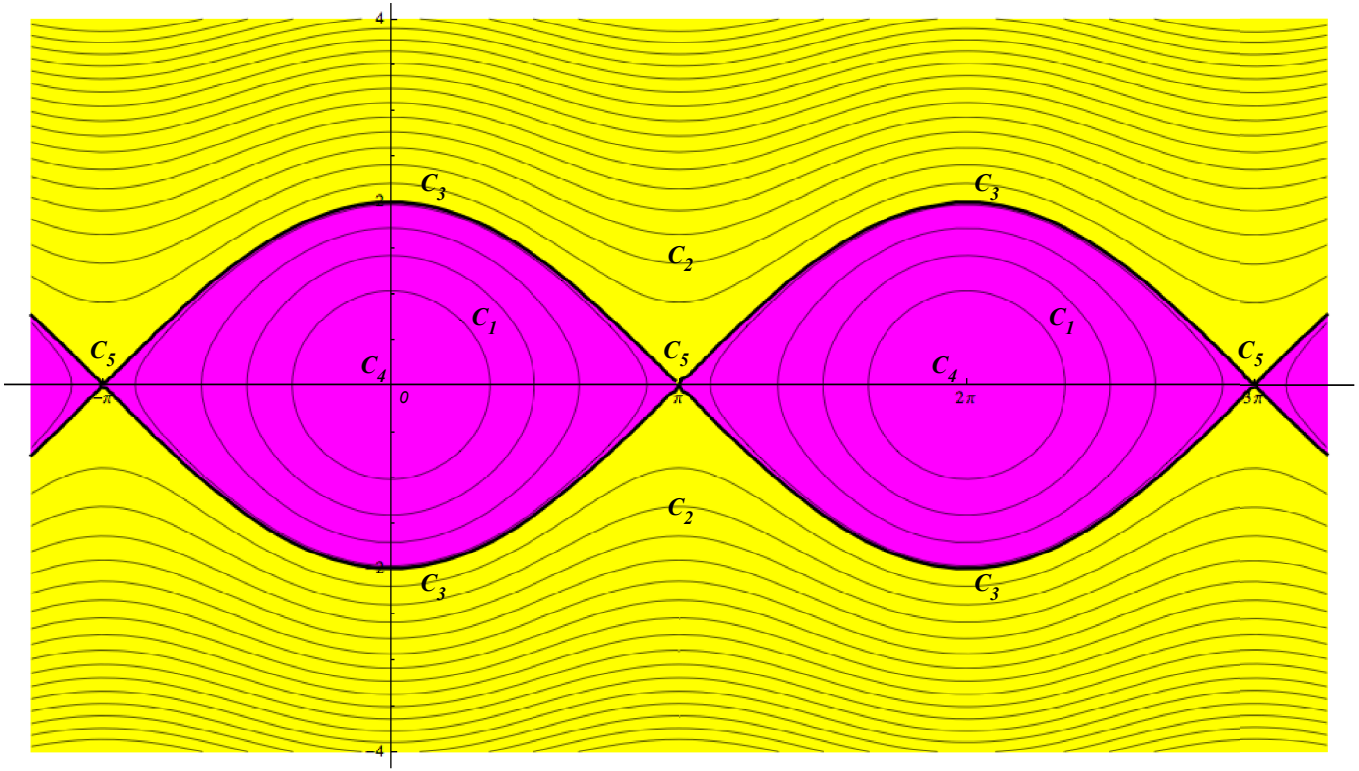

43. Jacobi coordinates

Sachkov then computes all the sub-Riemannian geometry of $\mathbb{V}_S = SE(2)$ using *Jacobi coordinates* (φ, k) which "rectify" the dynamics of the pendulum $\ddot{\gamma} = -\sin(\gamma)$.

In these coordinates, the "vertical" system in the fibers becomes trivial because $\dot{k} = 0$ and $\dot{\varphi} = 1$, i.e. $\varphi_t = \varphi + t$ with $\varphi = \varphi_0$. k is the modulus of the elliptic integral associated with the pendulum: it encodes the energy E; φ is the "pendular" time-length: it encodes the length of the geodesic.

44. $SE(2)$ geodesic equations

For the C_1^0 stratum, Moiseev and Sachkov find (with $x_t = x(t)$, etc., and $\mathbb{E}(\varphi) = \int_0^\varphi \mathrm{dn}^2(r,k)\,dr$):

$$\begin{cases} c = 2k\,\mathrm{cn}(\varphi,k) \\ \sin\left(\frac{\gamma}{2}\right) = k\,\mathrm{sn}(\varphi,k) \ \text{ and } \ \cos\left(\frac{\gamma}{2}\right) = \mathrm{dn}(\varphi,k) \\ \cos(\theta_t) = \mathrm{cn}(\varphi,k)\,\mathrm{cn}(\varphi_t,k) + \mathrm{sn}(\varphi,k)\,\mathrm{sn}(\varphi_t,k) \\ \sin(\theta_t) = \mathrm{sn}(\varphi,k)\,\mathrm{cn}(\varphi_t,k) - \mathrm{cn}(\varphi,k)\,\mathrm{sn}(\varphi_t,k) \\ x_t = \frac{1}{k}\left(\mathrm{cn}(\varphi,k)\left(\mathrm{dn}(\varphi,k) - \mathrm{dn}(\varphi_t,k)\right) + \mathrm{sn}(\varphi,k)\left(t + \mathbb{E}(\varphi) - \mathbb{E}(\varphi_t)\right)\right) \\ y_t = \frac{1}{k}\left(\mathrm{sn}(\varphi,k)\left(\mathrm{dn}(\varphi,k) - \mathrm{dn}(\varphi_t,k)\right) - \mathrm{cn}(\varphi,k)\left(t + \mathbb{E}(\varphi) - \mathbb{E}(\varphi_t)\right)\right) \\ \theta_t = \mathrm{am}(\varphi) - \mathrm{am}(\varphi_t) \mod (2\pi) \end{cases}$$

We have similar formulas for the other strata.

45. The SR spheres and wavefronts of $SE(2)$

The sub-Riemannian spheres $S(0,R)$ and wavefronts $W(0,R)$, $S(0,R) \subset W(0,R)$, of $\mathbb{V}_S = SE(2)$ look a bit like those of the polarized Heisenberg group, but are much more complicated.

The fundamental difference is that the y-axis, which was a degenerate caustic in the $\mathbb{V}_J$ case splits into four branches and the point singularities on it unfold into small "tetrapaks".

We illustrate the case $R = \frac{\pi}{2}$. The strata C_i are sent by the exponential map into strata $W_{C_i,\frac{\pi}{2}}$ of $W\left(0,\frac{\pi}{2}\right)$. The following figure displays $W_{C_1,\frac{\pi}{2}}$ as well as $W_{C_3,\frac{\pi}{2}}$.

46. $W_{C_1,\frac{\pi}{2}}$ and $W_{C_3,\frac{\pi}{2}}$

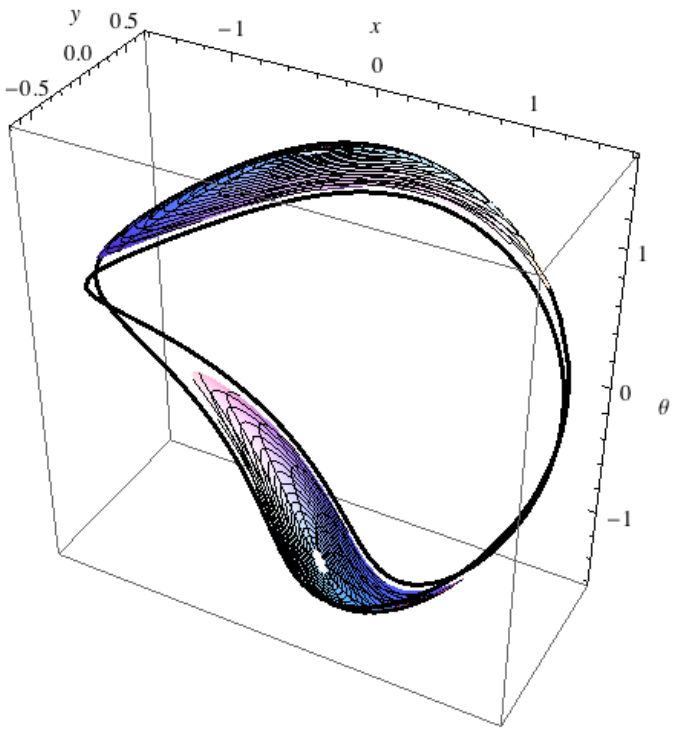

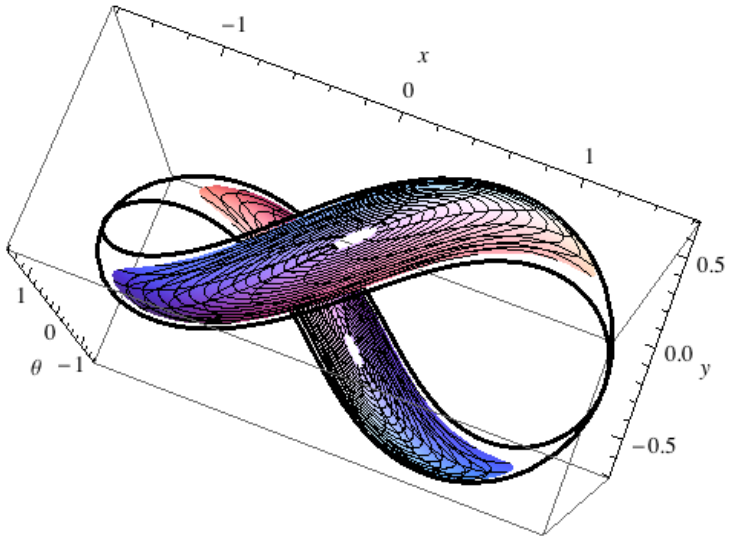

47. $W_{C_2^+,R=\frac{\pi}{2}}$

The images of the $C_2^{\pm}$ strata are much more complicated, with an infinity of singularities accumulating on the origin.

Let us consider the image $W_{C_2^+,\frac{\pi}{2}}$ of C_2^+ with its level lines L_k for $k = \text{cst}$. The figure shows some of them from two points of view. They are twisted circles with highly oscillating mean "radius".

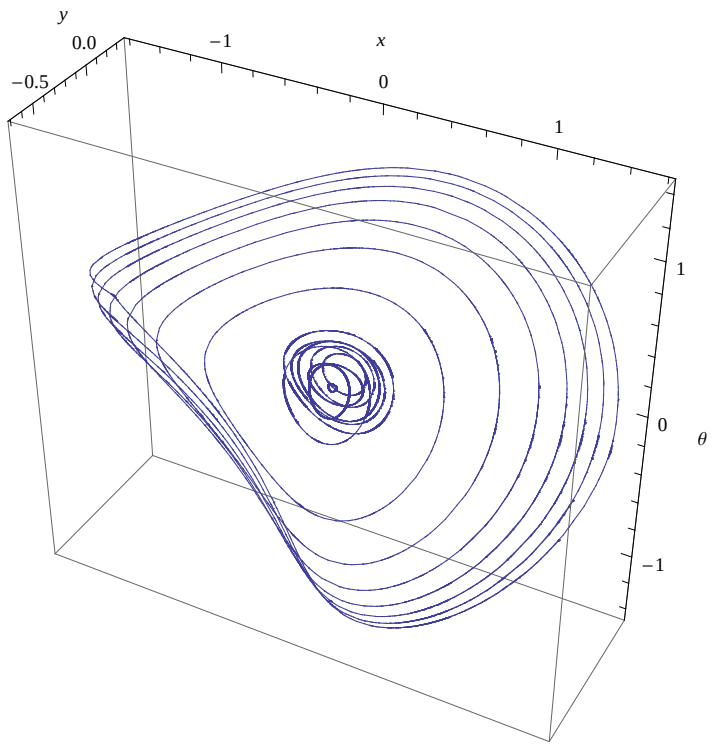

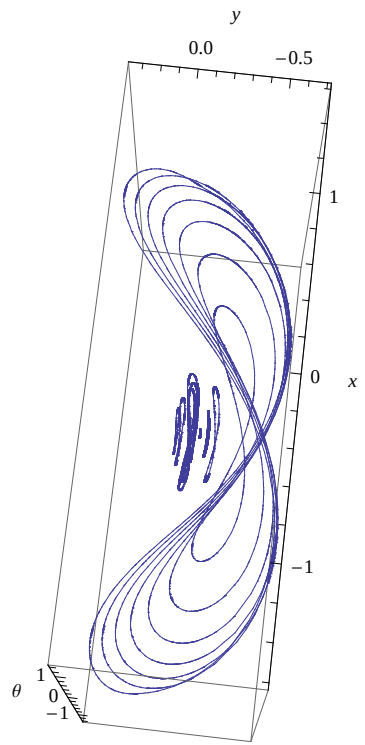

48. $W_{C_2^+,\frac{\pi}{2}}$

$W_{C_2^+,\frac{\pi}{2}}$ for $k \in (0.07, 0.8)$.

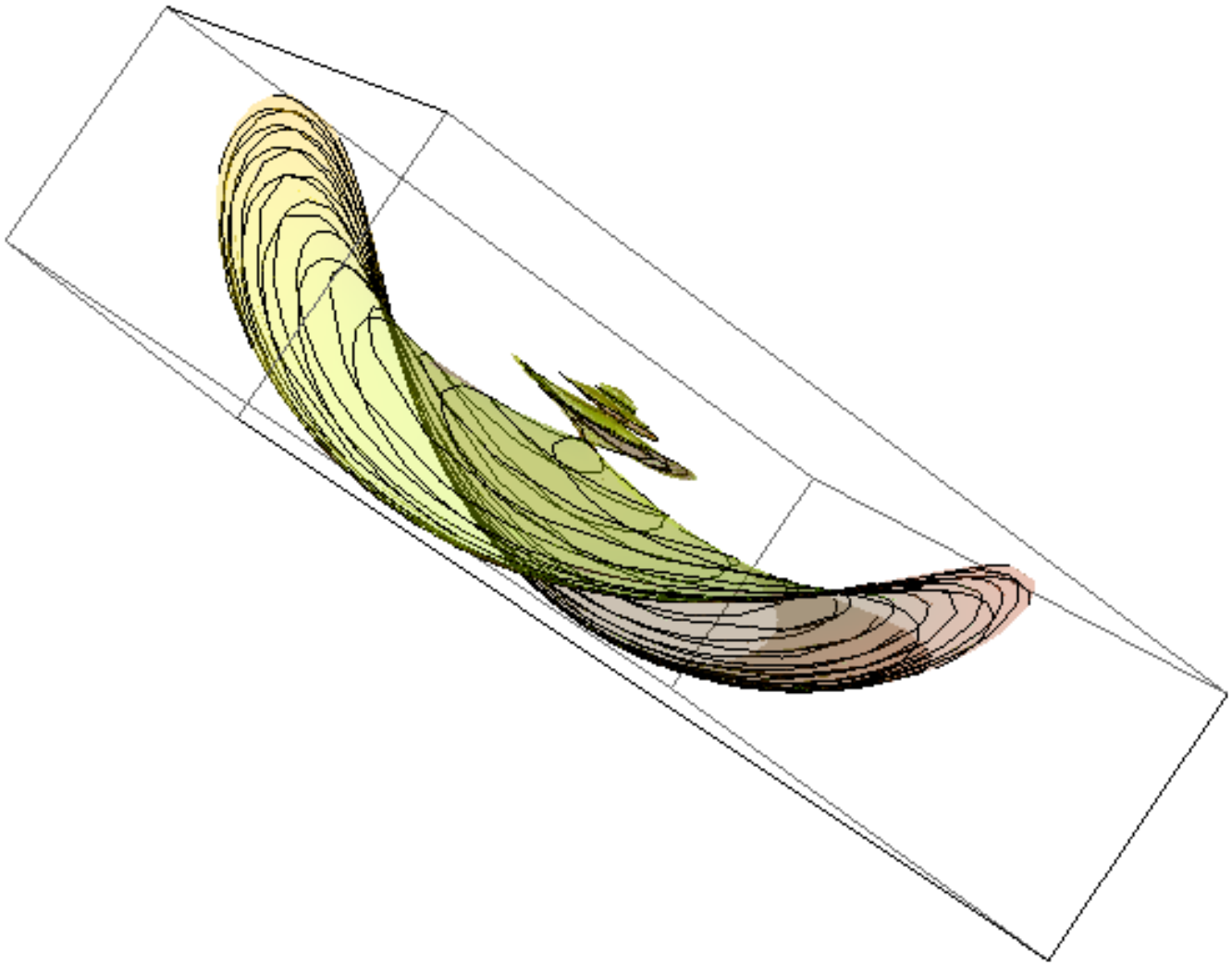

49. Exceptional level lines I

In the formulas for strata C_1 and C_2, the Jacobi elliptic functions have a period $T_1(k) = 4K(k)$ for C_1 and $T_2(k) = 4kK(k)$ for C_2. As $\varphi_t = \varphi + t$, then if $t = T(k) = R$, the formulas can be simplified.

For C_1, there exists a solution k_R only if $t \geq 2\pi$.

But for C_2 (e.g. C_2^+) there exists *always* a solution k_R of $t = R = 4kK(k)$ and then, for $k = k_R$, we get exceptional level lines.

And as $\operatorname{sn}(\varphi + 2K, k) = -\operatorname{sn}(\varphi, k)$ while $\operatorname{dn}(\varphi + 2K, k) = \operatorname{dn}(\varphi, k)$, the exceptional level line L_{k_R} is *degenerate* since y_R being of period only $2K$ takes twice the same value.

I made some pictures.

50. Exceptional level lines II

We have $k_{\frac{\pi}{2}} \sim 0.246139$. And we note then that, for $k_{c,\frac{\pi}{2}} \sim 0.2541$ neighbor of $k_{\frac{\pi}{2}} \sim 0.246139$, there exists another degenerate level line $L_{k_{c,\frac{\pi}{2}}}$. The geometry of the wave-front $W\left(0, \frac{\pi}{2}\right)$ between these values is particular because the L_k have an *envelope*.

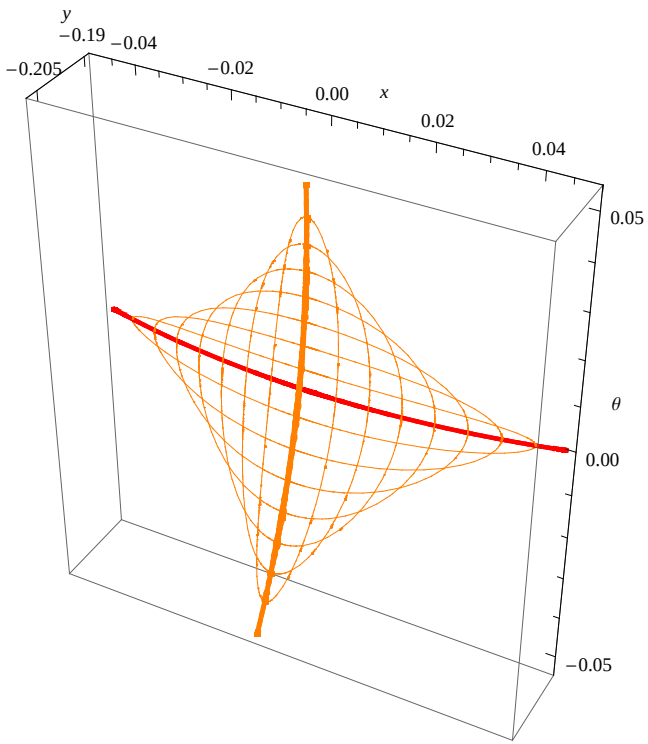

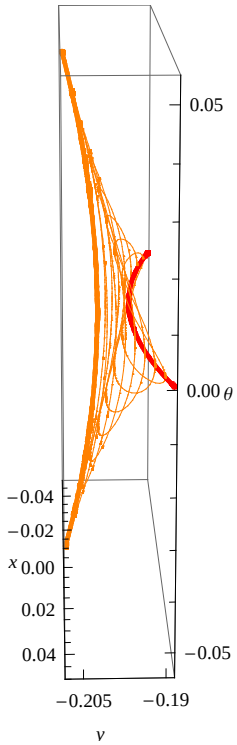

51. Intermediary "Tetrapaks"

This geometry of transition between L_{kR} and $L_{k_c,R}$ has the shape of a "tetrapak" of which a simple model is represented in the following figure

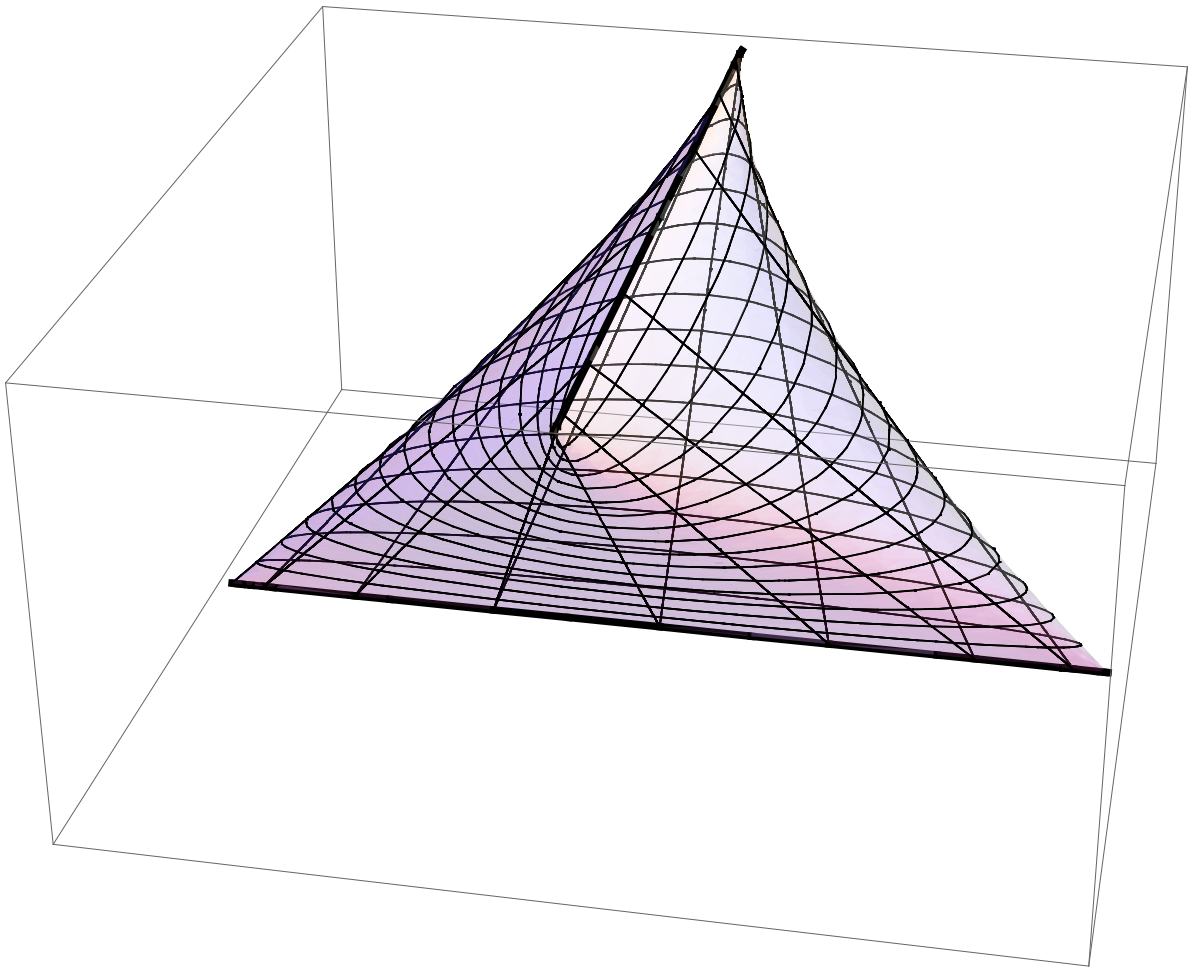

52. A "tetrapak" transition

The following figure shows the front $W\left(0, \frac{\pi}{2}\right)$ for $k \in [0.24, 0.26]$ with the "tetrapak" transition between the degenerate level lines $k_{\frac{\pi}{2}} \sim 0.246139$ and $k_{c,\frac{\pi}{2}} \sim 0.254126$.

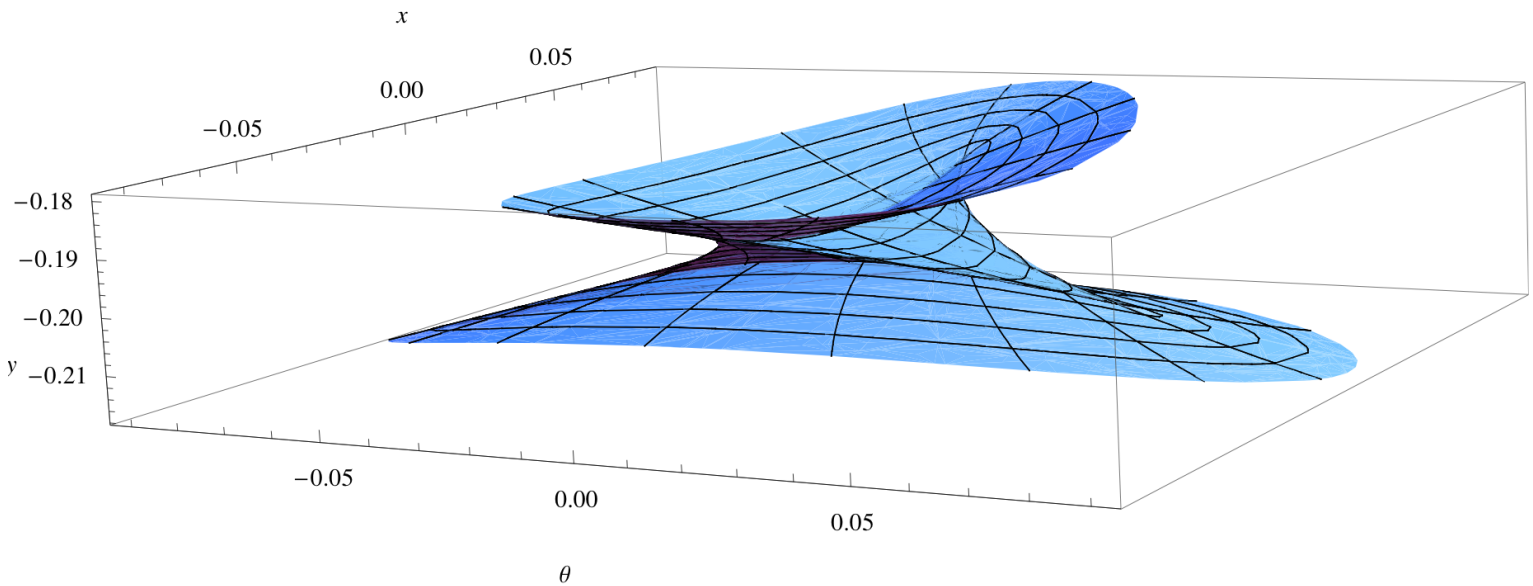

53. Caustic

When the radius R varies, the ends of the degenerate level lines L_{k_R} and $L_{k_{c,R}}$ run along four branches which split the y-axis of the Heisenberg case (caustic).

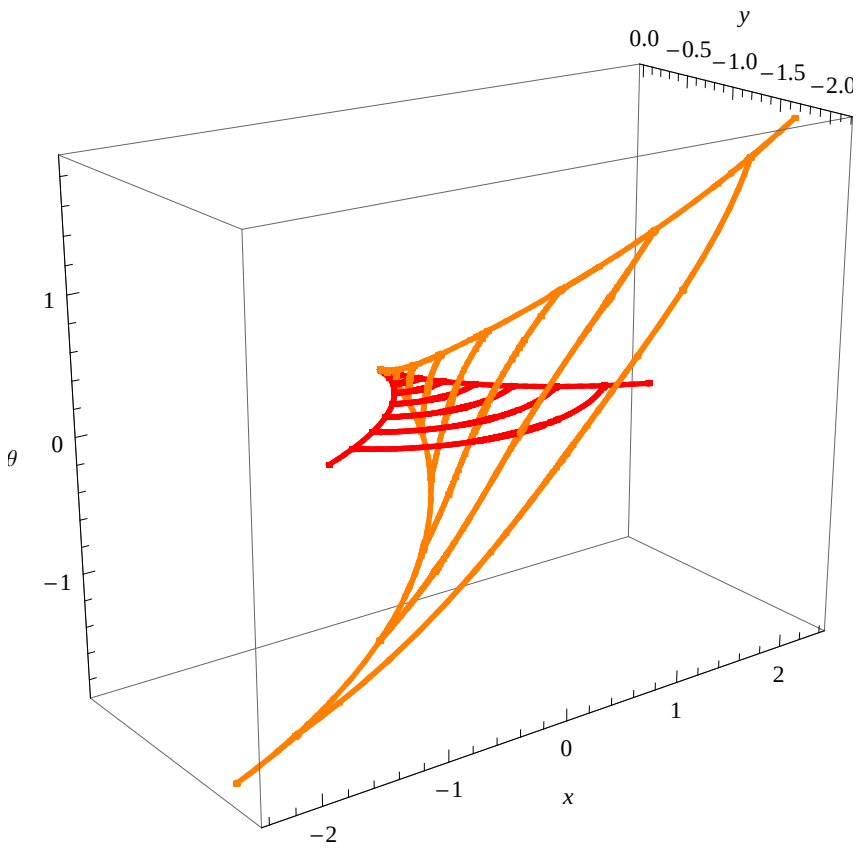

54. $SE(2)$ wave front

Next figure displays (with two points of view) the sphere $S\left(0, \frac{\pi}{2}\right)$ and the wavefront $W\left(0, \frac{\pi}{2}\right)$ for $k \leq 0.8$.

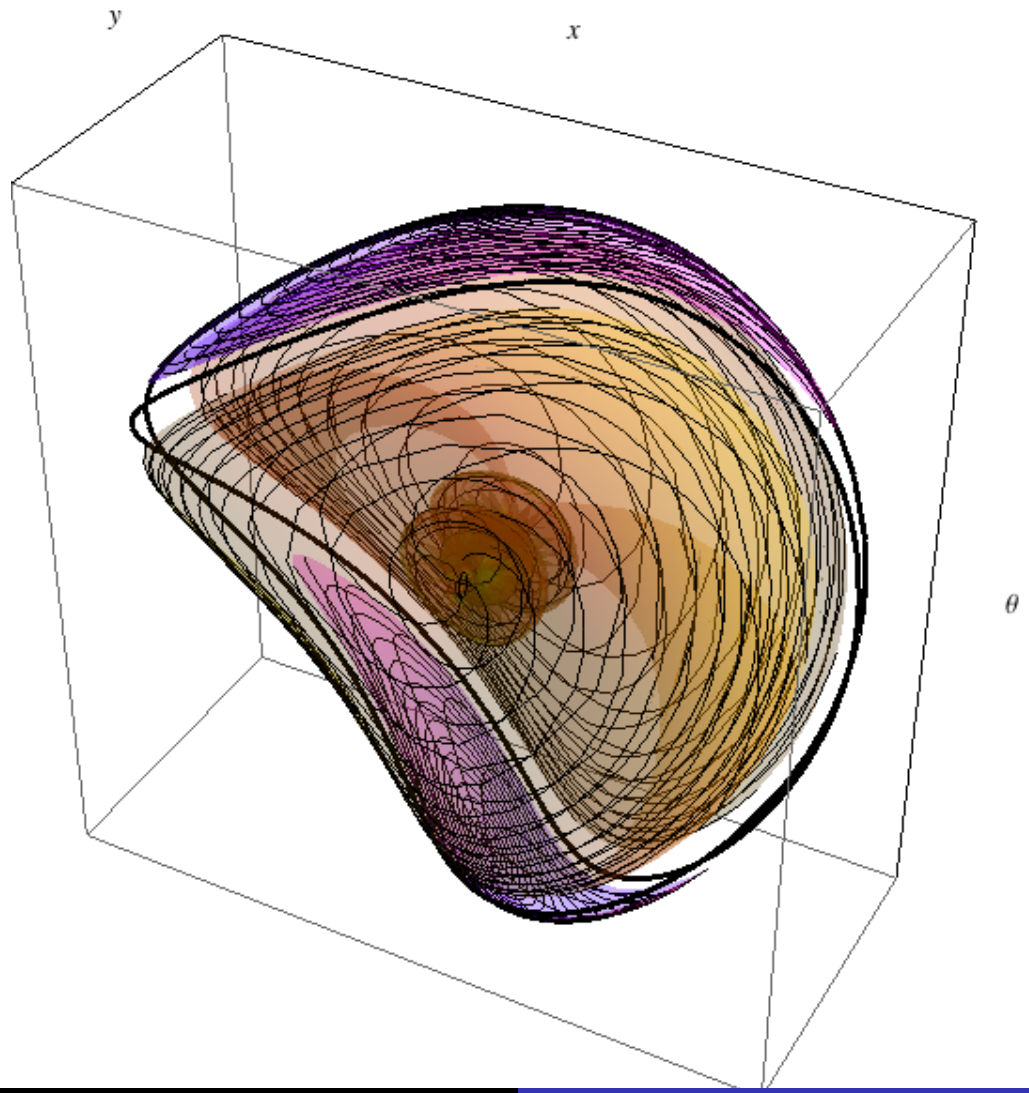

55. $SE(2)$ wave front

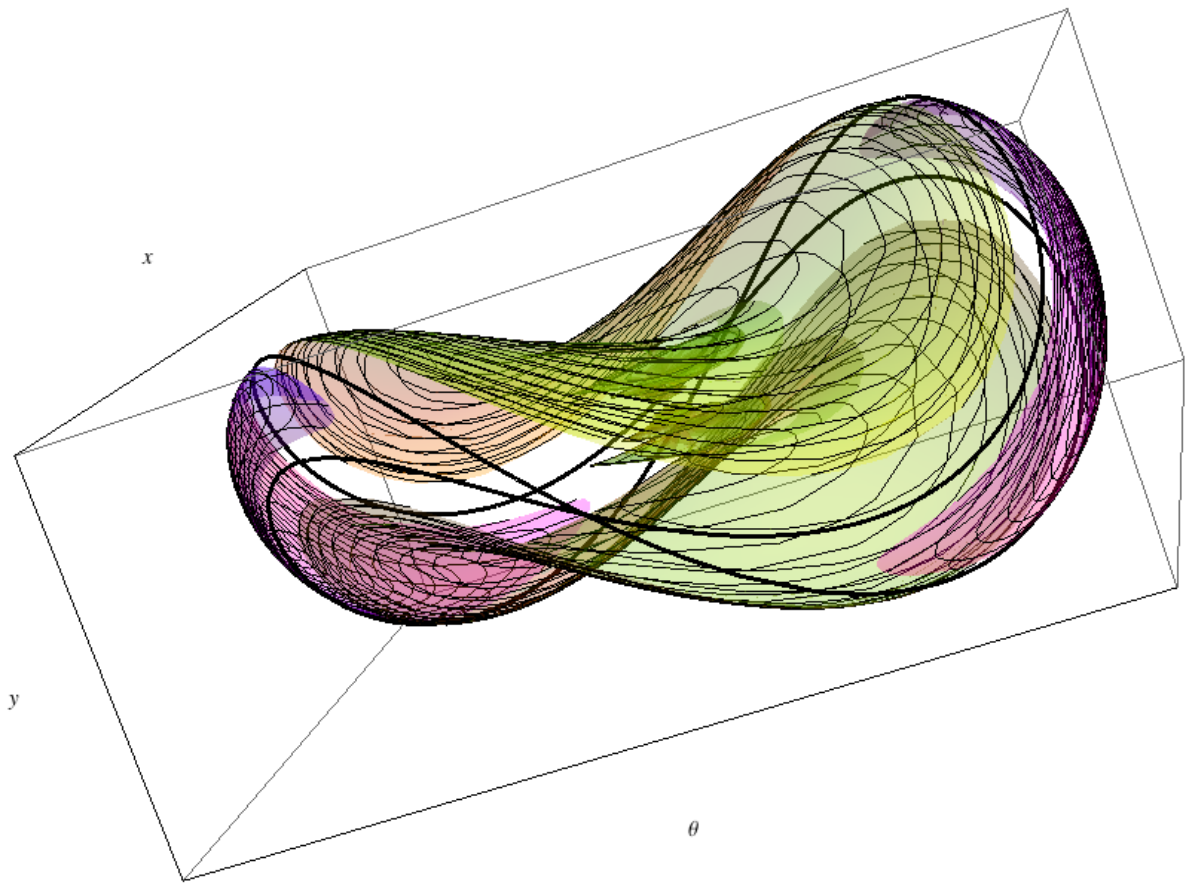

56. $SE(2)$ complexity

We see that the SR geometry of a Lie group as elementary as $SE(2)$ is rather complex.

57. Planets cannot compute

It is perhaps relevant to give here a completely different, but very well-known, example of a similar problem.

In the Newtonian theory of gravitation, we have the differential equations giving by integration the trajectories of the planets
(i) within the framework of a globally Euclidean space-time background structure (classical Galilean relativity), and
(ii) with the crazy hypothesis of long distance instantaneous forces.

But planets cannot "compute" anything: they can only follow *inertial* motions.

So, how can simple inertial motions be equivalent to complicated observed and computed trajectories?

58. Riemannian geometry can compute

How is it possible to explain gravitation purely locally and inertially?

It has been General Relativity that provided the solution by changing the globally Enclidean-Galilean background structure and using (semi-)Riemannian geometry.

Trajectories become geodesics and, in this new framework, can now be *at the same time* inertial and as complicated as needed to fit the empirical data.

59. Sub-Riemannian geometry can compute

It is the same thing here.

We observe complicated geometric structures of visual perception and we compute models using the Euclidean plane $\mathbb{R}^2$ as background structure (2D image processing).

But neurons cannot compute anything. They can only be active and propagate their activation along their connections.

Their connectivity must therefore be equivalent to differential computations.

To "achieve this goal", biological evolution (even if it is Darwinian and without "goal") has progressively implemented, in sophisticated modular connectivities, fiber structures of dimension $2 + n$ as jets, contact structures, and sub-Riemannian metrics ...

60. Inpainting and SR diffusion

I will conclude this presentation with the problem of *inpainting*, that is the completion of corrupted images.

It is natural to use *diffusion* along the horizontal connections, that is the sub-Riemannian hypoelliptic Laplacian $\Delta = X_1^2 + X_2^2$, and the sub-Riemannian heat kernel.

61. Lifting level sets and filling-in the gaps

Given an image of intensity function $I(x, y)$, we can consider the Legendrian lifts in $\mathbb{V}$ of its level curves.

We get a surface Σ in $\mathbb{V}$.

Let's suppose that the image is corrupted and contains a gap Λ.

To restore the image and to fill-in Λ, the idea is to use the *highly anisotropic* sub-Riemannian diffusion on $\mathbb{V}$.

The idea is conceptually simple but computationnally difficult.

62. Gauthier-Prandi inpainting

In their *SpringerBrief* on our sub-Riemannian neurogeometrical model (2018), Jean-Paul Gauthier and Dario Prandi deeply improved the computationnal efficiency of the model.

They used a *semi-discrete* version which is a left-invariant sub-Riemannian structure no longer over $SE(2)$ but over $SE(2, N)$ ($SE(2)$ restricted to a *finite* number of rotations).

In the following display, they start with an image almost completely concealed by a grid. The residual information is very sparse and scattered.

They apply sub-Riemannian diffusion until the grid has vanished.

Despite its dramatic corruption, the geometry of the initial image can be restored very correctly.

63. Inpainting image

Top-left: initial image, top-right: highly corrupted image, bottom: restored image.
(See also the exemple at the beginning of the talk.)

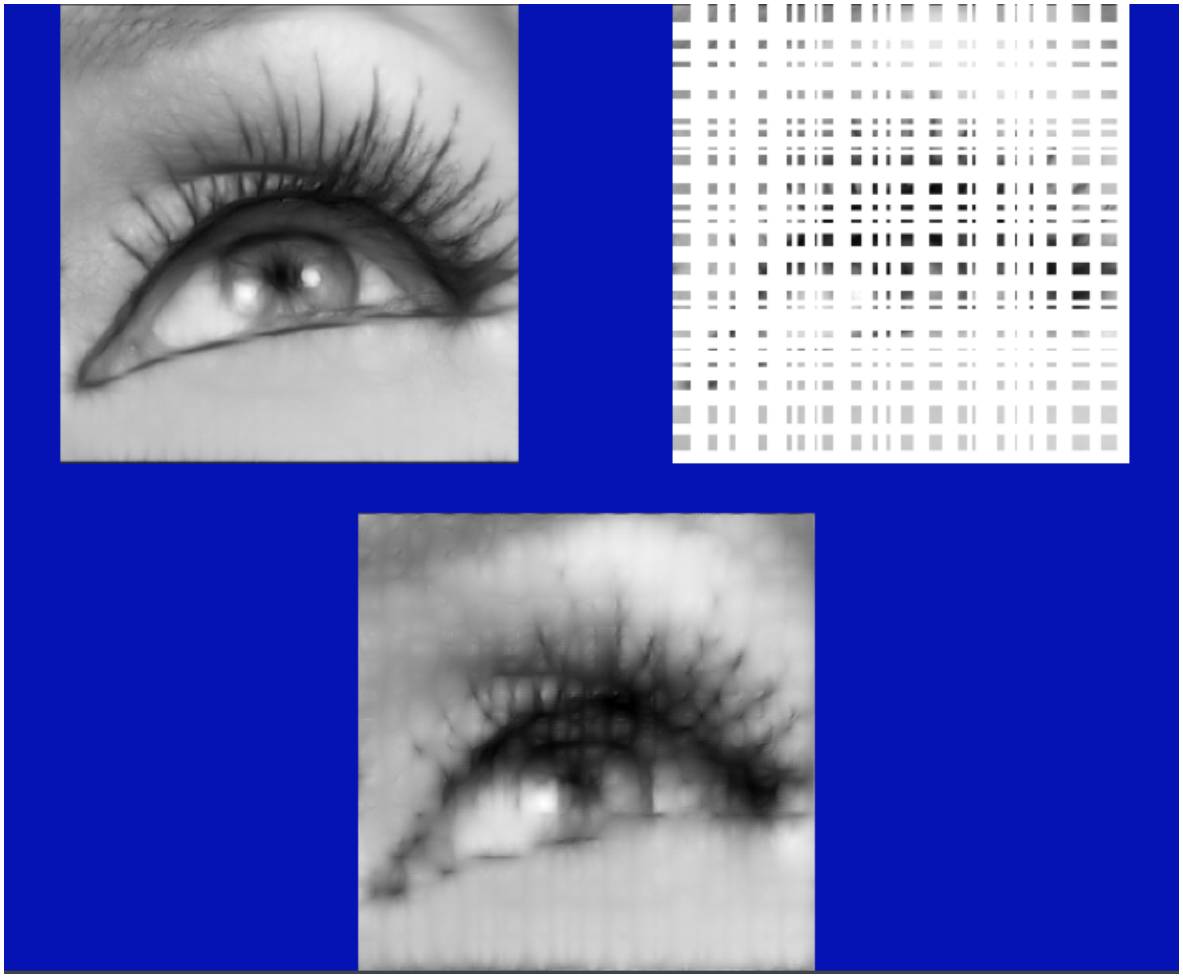

64. An active field

Today, geometric methods in neuroscience constitute a very active field.

E.g. recently (Winter 2017) Matilde Marcolli (who worked with Misha Gromov and Alain Connes) devoted with her colleague Doris Tsao a very nice course on such topics, in particular the use of contact geometry in Neurogeometry.

In March 2020, they co-organized a "Focus Program" at the Fields Institute (Toronto).

Here is the presentation of their course. Look at Gromov's quotation.

65. Geometry of Neuroscience at Caltech

"It is unimaginable that a viable representation of the brain/mind interface is possible without being incorporated into a broader mathematical framework."
-Mikhail Gromov, "Structures, Learning, and Ergosystems"